Available online at www.sciencedirect.com

SCIENCE DIRECT®

Remote Sensing of Environment 94 (2005) 463–474

Remote Sensing of Environment

www.elsevier.com/locate/rse

Combination of SRTM3 and repeat ASTER data for deriving alpine glacier flow velocities in the Bhutan Himalaya

A. Kääb*

Department of Geography, University of Zurich, Winterthurerstrasse 190, 8057 Zurich, Switzerland

Received 3 September 2004; received in revised form 4 November 2004; accepted 7 November 2004

Abstract

The present study evaluates the fusion of DEMs from the Advanced Spaceborne Thermal Emission and Reflection Radiometer (ASTER) instrument and the Shuttle Radar Topography Mission (SRTM). The study area consists of high elevation glaciers draining through the rough topography of the Bhutan Himalayas. It turns out that the ASTER-derived and SRTM3 DEMs have similar accuracy over the study area, but the SRTM3 DEM contains less gross errors. However, for rough topography large sections of the SRTM3 DEM contain no data. We therefore compile a combined SRTM3-ASTER DEM. From this final composite-master DEM, we produce repeat ASTER orthoimages from which we evaluate the DEM quality and derive glacier surface velocities through image matching. The glacier tongues north of the Himalayan main ridge, which enter the Tibet plateau, show maximum surface velocities in the order of 100–200 m year^{-1}. In contrast, the ice within the glacier tongues south of the main ridge flows with a few tens of meters per year. These findings have a number of implications, among others for glacier dynamics, glacier response to climate change, glacier lake development, or glacial erosion. The study indicates that space-based remote sensing can provide new insights into the magnitude of selected surface processes and feedback mechanisms that govern mountain geodynamics.

Keywords: TERRA-ASTER; SRTM; Digital elevation model; Fusion; Orthoprojection; Image matching; Glacier flow; Bhutan; Himalaya

1. Introduction

Mountain glaciers are especially sensitive to climate variations. As a result, the Intergovernmental Panel on Climate Change (IPCC) recognizes mountain glaciers as one of the top priority climate indicators (McCarthy et al., 2001). Due to the size and remoteness of most mountain glaciers, global-scale glacier monitoring relies heavily on satellite techniques. The international Global Land Ice Measurements from Space (GLIMS) initiative compiles a global glacier inventory and tracks glacier changes over time, mainly using Landsat and ASTER data (Bishop et al., 2004; Kieffer et al., 2000). Furthermore, in several high-mountain regions of the world ongoing climate warming markedly intensifies hazards related to glaciers, a fact that requires enhanced monitoring activities (Kääb et al., 2003c, 2005).

Ice flow is one of the basic processes of glaciers. Glacier geometry and extent is governed by the balance of mass flux into the system (accumulation, usually through snowfall) and out of the system (ablation, usually through ice melt), and by the ice transport within the system. A change in the climate can affect the mass balance, which represents the direct climate signal, and the ice dynamics of the glacier. For example in the Swiss Alps, an increasing number of glaciers are currently downwasting (i.e. stationary decaying) instead of retreating in response to atmospheric warming (Paul et al., 2004), because the ice melt by far overrules the mass supply through accumulation and ice flow. As a second example, ice flow is a crucial factor in the evolution of sometimes dangerous ice-contact lakes which develop under the imbalance between ice melt at the ice front and ice supply from flow. The surface velocity field of glaciers is thus an important glaciological parameter for glacier inventorying and monitoring, and glacier hazard assessments.

* Tel.: +41 1 635 51 46; fax: +41 1 635 68 48.
E-mail address: kaeaeb@geo.unizh.ch.

0034-4257/$ - see front matter © 2004 Elsevier Inc. All rights reserved.
doi:10.1016/j.rse.2004.11.003

Remote sensing techniques are commonly used to determine ice flow velocities for remote glaciers. These techniques include microwave data (e.g. differential interferometric synthetic aperture radar, DInSAR; e.g. Rignot et al., 1996) and optical imagery (e.g. image matching; for references, see the below chapter on image matching). The focus of the present study is to use repeat optical satellite imagery to collect ice velocity measurements. In order to measure surface displacements from repeat imagery, the following conditions must be met:

- Surface features have to be detectable in at least two of the repeat optical data sets in order to track them.
- The multitemporal data sets have to be accurately co-registered. For the rough topography found in the study area, this condition requires a terrain correction of the repeat imagery.
- The spatial resolution of the image data has to be finer than the displacements, in order to obtain results at a statistically significant level.

The Advanced Spaceborne Thermal Emission and Reflection Radiometer (ASTER) with its stereo band, and the DEM obtained from the Shuttle Radar Topography Mission (SRTM) provide a nearly global multi-resolution data base for deriving glacier flow fields by optical techniques. In the present study, this potential is exploited for the main ridge of the Bhutan Himalayas (Figs. 1 and 2).

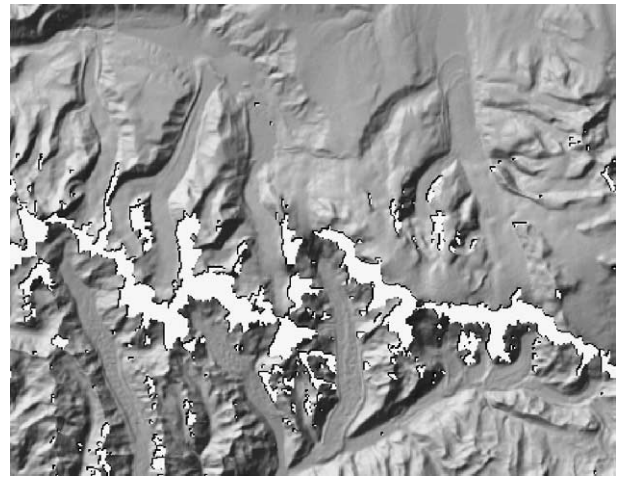

Fig. 2. Hillshade of the SRTM3 DEM of the study area. White regions indicate data gaps in the original data.

The center of the study area is the northernmost section of the Bhutan Himalayan main ridge (called "Lunana"; roughly 28°N, 90–91°E; Gansser, 1970) separating the Tibet plateau to the north from the central Himalayas to the south (Fig. 1). The lowest terrain parts studied of about 3700 m a.s.l. lie in the valleys south of the main ridge. The northern sections towards the Tibet plateau show minimum elevations of around 5000 m. Highest peaks are around 7300 m. Thus, the study area represents one of the highest mountain relieves found on Earth.

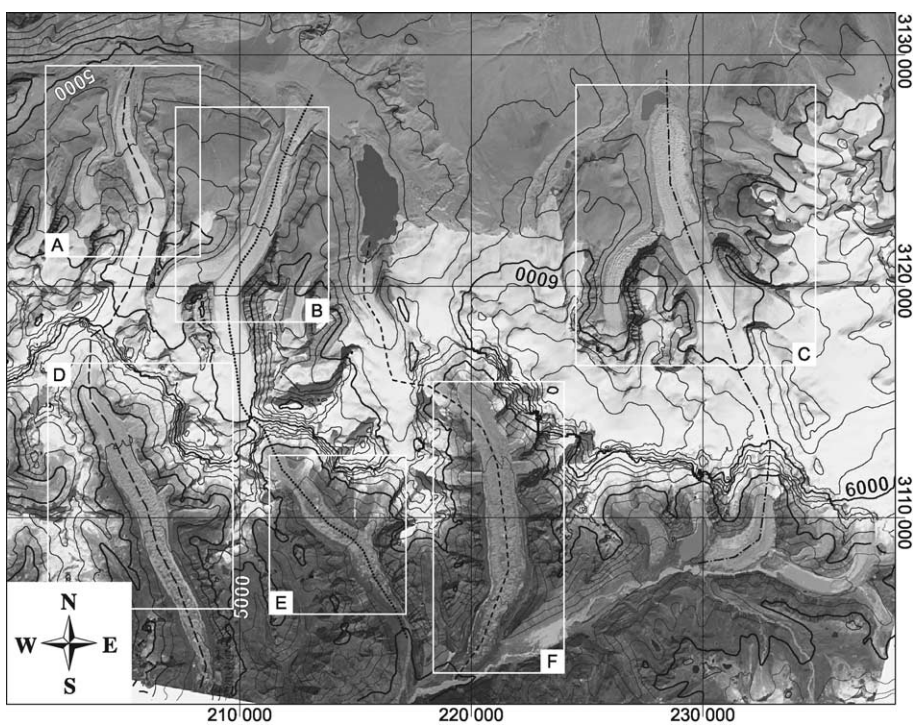

Fig. 1. Orthoprojected ASTER image from 20 November 2001 showing a section of the Bhutan Himalayas main ridge. The 200 m contour lines are from a combined SRTM3-ASTER DEM. The rectangles with letters A–F indicate the image sections shown in Fig. 7. The lines following the glacier center lines mark the locations of the elevation profiles in Fig. 8. Coordinates are in WGS84 UTM Zone 46.

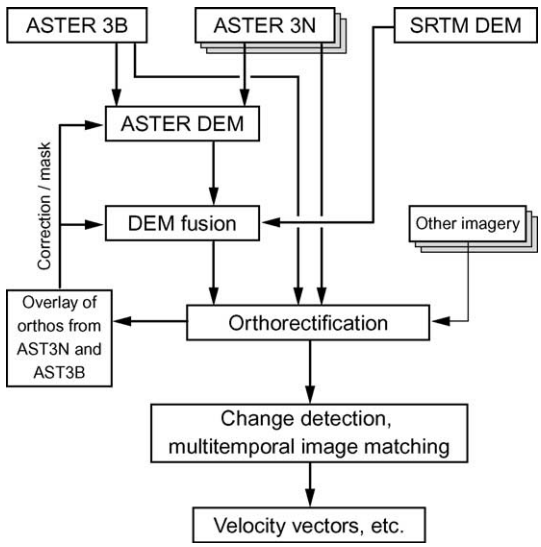

Fig. 3. Image processing scheme used for the present study.

Most northern glaciers are directed to the north, most southern glaciers to the south. The glacier tongues we investigate are found at minimum elevations of 5000 m to the north, and 4000 m to the south of the main Bhutan watershed. Eighty to ninety percent of the total annual precipitation in the southern valleys (Lunana; 500–700 mm year^{-1}) falls during March to October (Meyer et al., 2003; see also Karma et al., 2003; Mool et al., 2001). Floods from glacier lake outburst are one of the severest natural hazards in Lunana and among the most important processes of sediment redistribution and evacuation in the area (Ageta et al., 2000; Gansser, 1970; Mool et al., 2001; Watanabe & Rothacher, 1996).

In this work, we topographically correct multitemporal ASTER data of the study area using a combined DEM from SRTM and ASTER data. Digital matching of the repeat ASTER orthoimages is used to derive glacier flow fields (cf. Fig. 3). First, the study intends to evaluate a methodology for satellite-based inventorying and monitoring of ice flow for a large number of glaciers. Second, data about glacier dynamics in a so far little studied and hardly accessible mountain range is presented.

2. Digital elevation models

Accurate DEMs are necessary for topographic correction and co-registration of multitemporal satellite images, which are usually taken with different incidence angles (Fig. 3). The SRTM DEM and DEMs generated from ASTER stereo data have a large global coverage and are therefore used here.

2.1. The SRTM3 DEM

The single-pass InSAR SRTM campaign of February 2000 provides a unique DEM for large sectors of the continents (60°N–54°S, e.g. Van Zyl, 2001). The SRTM DEM is available in two spatial resolutions: SRTM1 with 1 arc sec (approximately 30 m) and SRTM3 with 3 arc sec (approximately 90 m). Vertical reference of the SRTM DEMs is the WGS84 EGM96 geoid. The mission report quotes a DEM resolution of several tens of meters, an absolute vertical accuracy of ±16 m (linear error at 90% confidence level, LE90), a relative vertical accuracy of ±6 m (LE90), and a horizontal positional accuracy of about ±20 m (circular error, CE90) (Rabus et al., 2003).

Initial assessments of the SRTM DEMs show that the mission specifications were well fulfilled (Rignot et al., 2003; Sun et al., 2003). Strozzi et al. (2003) compared the SRTM1 DEM to an automatic aerophotogrammetric DEM (Kääb, 2004; Strozzi et al., 2004) at Gruben, a high-elevation mountain site in the Swiss Alps. They obtained an average height difference of 7 m, a standard deviation of height difference of 36 m, and maximum errors of up to 285 m. Kääb (2004) compared the SRTM3 DEM with automatic aerophotogrammetric DEMs for the same test site and found a standard deviation of the height difference of ±20 m (RMS), with maximum vertical deviations of −193 and +143 m. For a subsection of the test area with moderate topography, the standard deviation of elevation differences was ±12 m, with maximum vertical deviations of −54 and +41 m. The cumulative histogram in Fig. 4 (right panel) suggests that a DEM derived from ASTER satellite stereo imagery (see following section) is competitive with the SRTM3 DEM for about 60–70% of the points. The SRTM3 DEM, however, includes significantly fewer large errors.

Kääb (2004) also evaluated the SRTM3 DEM for the tongue of Glaciar Chico in the Southern Patagonia Icefield. For this low relief site, the standard deviation for height differences between the aerophotogrammetric DEM (Kääb, 2004; Rivera et al., in press) and the SRTM3 DEM is ±15 m, with maximum deviations of 150 m. The cumulative histogram of vertical deviations (Fig. 4) reveals a better SRTM3 DEM compared to the ASTER DEM. However, at the time of acquisition, large sections of the only ASTER scene available for Glaciar Chico were snow-covered, which complicated the corresponding DEM generation.

The studies summarized above suggest that the SRTM3 DEM accurately resolves both high- and medium-relief terrain. For the study site in the Bhutan Himalayas, however, the SRTM3 DEM shows large sections without data, presumably a consequence of radar shadow, layover and insufficient interferometric coherence (Fig. 2). In order to produce a DEM with larger coverage, data fusion between the SRTM3 DEM and an ASTER DEM is necessary.

2.2. DEM from ASTER stereo

ASTER imagery has been used for global observation of land ice since 2000. The spectral and geometric capabilities of ASTER imagery include three bands in the VNIR (visible and near infrared) with 15 m resolution;

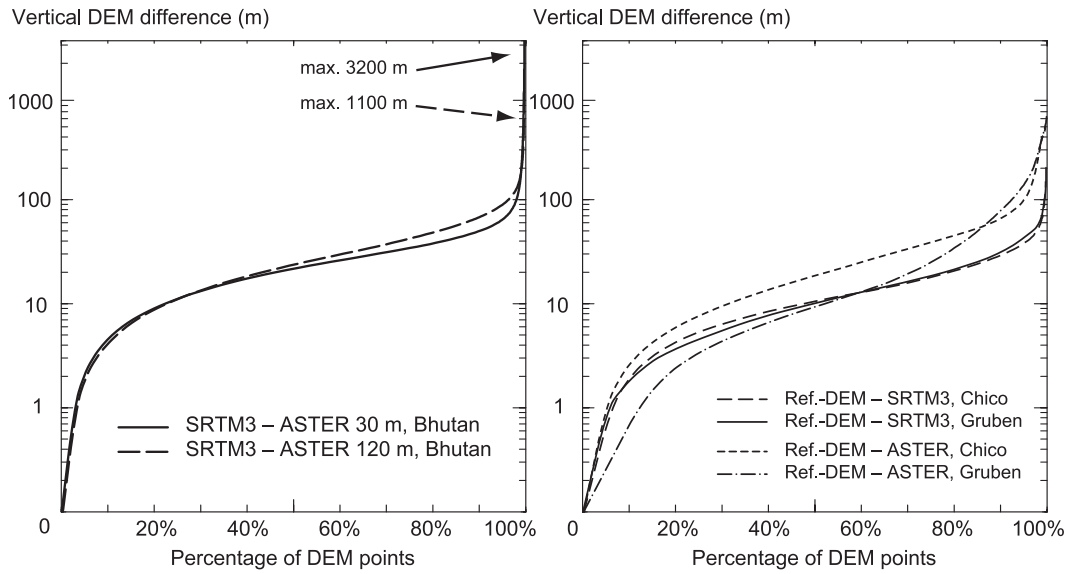

Fig. 4. Cumulative histograms of vertical differences between SRTM3, ASTER and aerophotogrammetric DEMs for the study site discussed here (left panel) and two other sites, Gruben, Swiss Alps, and Glaciar Chico, Chile (right panel). (Bhutan 30 m: 100%=201 000 points; Gruben ASTER: 100%=37 100 points; Gruben SRTM: 100%=4760 points; Chico ASTER: 100%=71 700 points; Chico SRTM: 100%=29 000 points).

six bands in the SWIR (short-wave infrared) with 30 m resolution; five bands in the TIR (thermal infrared) with 90 m resolution; and a 15 m resolution NIR along-track stereo-band looking 27.6° backwards from nadir. The stereo band (3B) covers the same spectral range of 0.76–0.86 μm as the nadir band (3N). The ASTER swath width is 60 km, but a swath of over 180 km can be produced by rotating the sensor ±8.5° cross-track (±24° possible for VNIR).

We generate a DEM of the study region using ASTER imagery from 20 November 2001. Orientation of the 3N and corresponding 3B bands, transformation to epipolar geometry, parallax-matching, and parallax-to-DEM conversion is done using the PCI Geomatica 8.0 Orthoengine software (Toutin & Cheng, 2001). No sufficient maps or other sources of ground control are available for the study region in Bhutan. The scene's geolocation included in the ASTER image-file header can be used for retrieving this information (Kääb, 2002). However, in order to ensure an optimal co-registration between the ASTER data and the SRTM3 DEM, control points (CPs) are transferred from the SRTM3 DEM to the ASTER images. The horizontal position of distinct terrain marks such as river junctions or peaks, identifiable in both the ASTER imagery and the SRTM data, is taken from a SRTM3 DEM hillshade (Fig. 2). The elevation of these ancillary CPs is also extracted from the SRTM3 DEM. Approximately 30 CPs are chosen resulting in an average horizontal error of ±30 m (RMS). This accuracy describes the quality of three-dimensional co-registration (i.e. relative accuracy) between the ASTER and SRTM data, not the accuracy of absolute position. Deriving glacier flow fields from repeat image data requires relative accuracy between the individual data layers, not the absolute accuracy of the entire data set.

Within the DEM assessment studies of Gruben and Glaciar Chico mentioned above, different ASTER DEMs were also compared to aerophotogrammetric reference DEMs (see also Kääb, 2004; Kääb et al., 2003a; Zollinger, 2003). For Glaciar Chico, the standard deviation for vertical differences between the aerophotogrammetric DEM and the ASTER DEM was ±31 m (RMS). For Gruben, the accuracy was ±70 m RMS. Maximum errors ranged between −200 and +500 m. For a subsection with moderate topography, an accuracy of ±20 m RMS and maximum errors of 100 m were found. (For other ASTER DEM evaluations, see, e.g. Hirano et al., 2003; Toutin, 2002).

All above numbers refer to ASTER DEMs generated with 30 m resolution (2 image pixels). In addition, ASTER DEMs with 120 m grid spacing (8 image pixels) are computed for the study region in Bhutan.

2.3. DEM merging and evaluation

Comparison between the SRTM3 DEM, and the ASTER 30 and 120 m DEMs for the Bhutan site show that the ASTER 120 m DEM includes significantly less gross errors than the ASTER 30 m DEM (Fig. 4, left panel). As a result, data gaps in the SRTM3 DEM (Fig. 2) are filled with the ASTER 120 m DEM. DEM merging is done by replacement of SRTM3 no-data cells with the corresponding ASTER DEM cells. For that purpose, both the ASTER DEM and the SRTM3 DEM are projected in UTM and resampled to 90 m. Contour lines of the resulting composite-master DEM are shown in Fig. 1.

For the Bhutan Himalayas and many other regions, generated DEMs cannot be tested against existing reference DEMs. Instead, two (or more) orthoimages from different sensor positions must be compared to each other (e.g.

Baltsavias, 1996). If the DEM is correct, the corresponding image pixels will perfectly overlap (Fig. 5). Vertical DEM errors, on the other hand, translate into horizontal shifts between the orthoprojected pixels of the source images (Fig. 5; Aniello, 2003).

For the Bhutan study area, orthoimages are computed based on the combined SRTM3-ASTER DEM. The horizontal projection shifts between the 3N and 3B ASTER orthoimages are visualized by a normalized difference index (NDI) between the two orthoimages ((AST3N-AST3B)/(AST3N+AST3B), where AST is the digital number (DN) of ASTER pixels in bands 3N or 3B; Fig. 6). Bright and dark areas in the NDI image indicate significant differences between the two orthoimages. These differences indicate the projection shifts that we investigate, but can also be caused by the bidirectional reflectance distribution function (BRDF; a surface point may show different reflectance if viewed from different positions, here 3N and 3B, even if the illumination is constant as may be assumed for the 55 s time lag between 3N and 3B acquisition). Independent of illumination, it is possible for north-facing slopes to be entirely hidden from view of the backward-looking sensor. For these zones and areas with no spatial variation in reflectance, no useful difference can be detected in the orthoimages, irrespective of DEM errors and corresponding projection shifts. The largest differences between the ASTER 3N and 3B orthoimages appear in areas with especially rough topography such as high peaks and steep walls where the largest DEM errors are in fact expected. In these zones, the elevation values originate, for the most part, from the ASTER 120 m DEM (cf. (Figs. 1, 2 and 6)).

More useful than NDIs or other image algebra is the animated overlay of the 3N and the 3B orthoimages. Horizontal projection errors between the orthoimages are easy to find through image flickering (Kääb et al., 2003b).

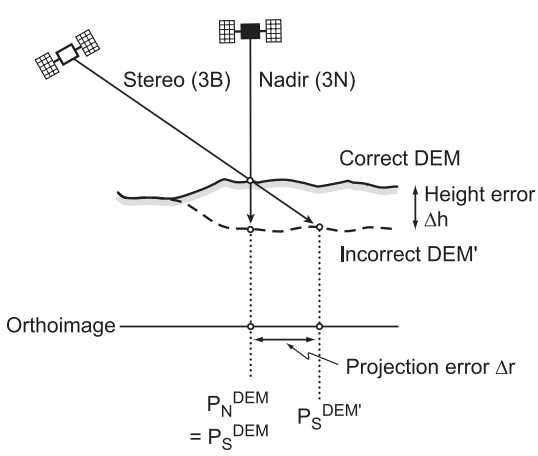

Fig. 5. Vertical errors of a DEM lead to horizontal shifts in the orthoprojection. The magnitude of these shifts is proportional to the DEM error and the incidence angle of the imagery applied with respect to the nadir direction. Thus, DEM errors can be explored by comparing orthoimages computed from images with different incidence angles, e.g. ASTER 3N and ASTER 3B (cf. Fig. 6).

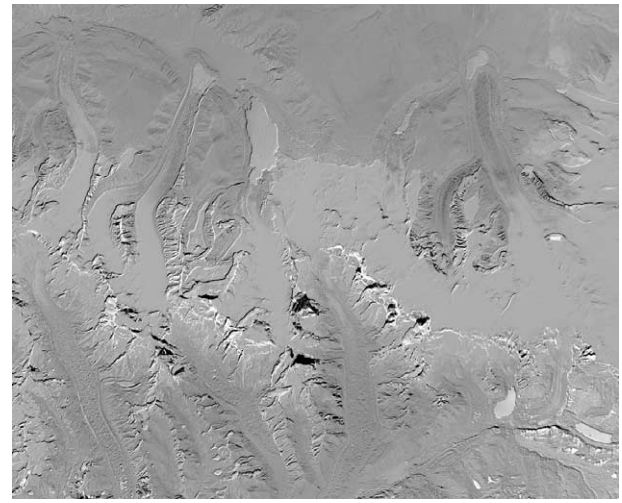

Fig. 6. Normalized difference image between two orthoimages of 20 November 2001, one computed from the ASTER nadir band 3N, the other from the backwards-looking ASTER band 3B. Bright and dark zones indicate among others sections with large horizontal shifts between the orthoimages from vertical DEM errors. The DEM used for orthoprojection was merged from the SRTM3 and ASTER DEM.

The composite-master DEM is evaluated using this technique and the NDI method. There are no significant DEM errors where ice velocities are later measured. Correction or masking out of erroneous DEM sections seems unnecessary in these zones. If DEM errors need to be corrected, this can be done either within the original DEM production process, or by transforming the horizontal projection shifts between multi-incidence-angle orthoimages into vertical elevation corrections (cf. Figs. 3 and 5) (e.g. Norvelle, 1996). The image matching technique presented in the following section can be used to automatically measure these horizontal shifts.

3. Image matching

An efficient method for extracting ice velocity is by tracking the displacement of features in repeat optical imagery (e.g. Bindschadler et al., 1994, 1996; Evans, 2000; Frezzotti et al., 1998; Kääb, 2002; Lefauconnier et al., 1994; Lucchitta & Ferguson, 1986; Rolstad et al., 1997; Scambos et al., 1992; Skvarca et al., 2003; Whillans & Tseng, 1995). Here, we derive the horizontal displacements of individual glacier features from multitemporal ASTER orthoimages using the Correlation Image Analysis Software CIAS (Kääb, 2002; Kääb & Vollmer, 2000). A double cross-correlation function based on grey values of the images is used to identify corresponding image blocks.

For the Bhutan study area, ASTER 3N bands from 20 January 2001, 20 November 2001 and 22 October 2002 are geocorrected using arbitrary CPs transferred from the SRTM3 DEM (see section above; Fig. 2). The three ASTER scenes used represent the most suitable data available by the time of the study in terms of spatial coverage, clouds and

snow cover. In order to avoid distortions between the multitemporal products, all imagery is adjusted as one image block connected by multitemporal tie-points—placed on stable terrain (i.e. outside the glaciers). Orthoprojection is based on the composite-master DEM. Velocity fields are derived for six glacier ablation areas (Fig. 7, see following section). Due to the lack of suitable optical glacier features, few velocity vectors can be measured on the other glacier zones.

Matching-blunders are eliminated using the individual correlation coefficients and constraints, such as the expected range for flow speed and direction. Statistical analysis of the noise within sections of coherent ice flow (Fig. 7) and previous accuracy assessments (Kääb, 2002, 2004; Kääb &

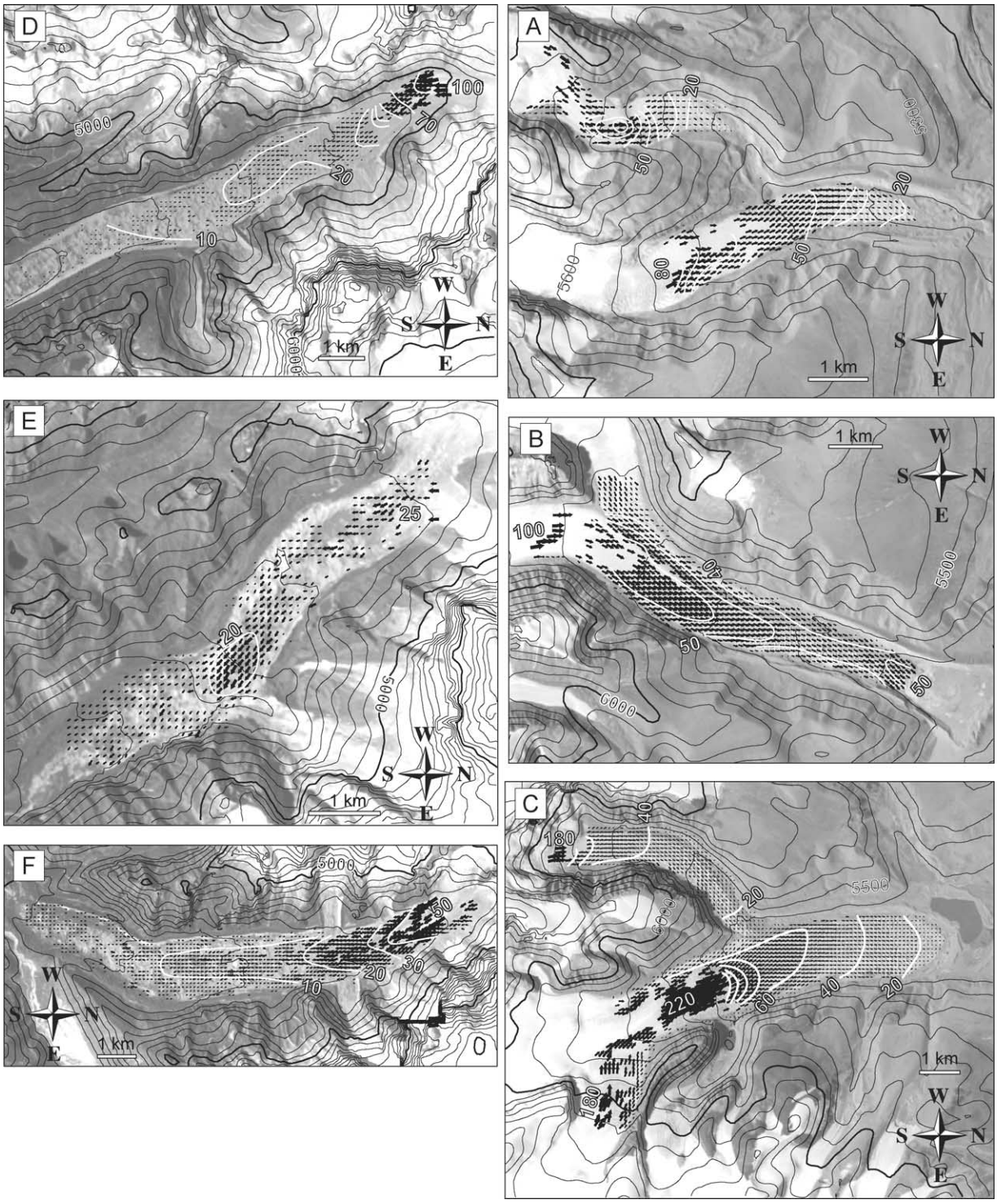

Fig. 7. Glacier surface flow fields 20 January–20 November 2001 for the image sections of Fig. 1. White isolines indicate the glacier speed.

Vollmer, 2000) predict an RMS error of 0.5–1× the image pixel size for the horizontal displacement measurements, i.e. 8–15 m for ASTER.

4. Glacier flow fields

Fig. 7 shows surface velocity fields derived between 20 January 2001 and 20 November 2001. Since most of the glaciers have no published name, the present results refer to image sections A–F (cf. Fig. 1). Sections A–C are located on the northern slope of the Bhutan Himalayas main ridge, sections D–F on the southern slope.

Two glacier tongues are situated in section A, both with no debris cover except for the snout area. For both glaciers, horizontal surface velocities of close to 90 m year^{-1} are found. The speed continuously decreases towards the terminus with sharp transverse gradients at the glacier margins. The displacement measurements rely predominantly on crevasses preserved throughout the measurement period. Velocities are also measured for November 2001–October 2002 and January 2001–October 2002 (not shown). Speeds during January 2001–November 2001 are roughly 10–20% faster than during November 2001–October 2002 for the eastern glacier in section A. However, this change is only slightly significant taking into account the measurement accuracy.

The glacier tongue in section B (Fig. 7) has only sparse debris cover. Again, the displacement measurements rely on crevasses, which are well preserved over the observational period. The velocity decreases from 100 to 40 m year^{-1} towards the terminus. There is a zone of acceleration above the calving glacier front. Ice velocity on the eastern tributary is about 30% higher than on the western one. Sharp transverse velocity gradients exist towards the glacier boundary but are otherwise small on the glacier. The calving front retreated by up to 150 m between January 2001 and November 2001, and by up to 110 m between November 2001 and October 2002. The maximum total retreat for January 2001 to October 2002 is 220 m. No statistically significant changes in speed are observed during this time period.

The glacier tongues in section C exhibit little debris cover, similar to the other northbound glaciers investigated. Absence of crevasses and other trackable features cause data gaps. The ice velocity is up to 220 m year^{-1} on the main branch and 180 m year^{-1} on the western branch. The high speed zone on the main tongue is related to a steep glacier section. The glacier decelerated by roughly 30% between the first image pair (January 2001–November 2001) and the second image pair (November 2001–October 2002).

The southbound glacier tongue in section D is heavily debris covered with a rough surface topography caused by differential melt. In contrast to the northbound glaciers, the measurements rely on topographic features and marked contrasts in the debris cover. For large parts of the glacier tongue surface speeds are below 20 m year^{-1}. In these parts, gaps in the velocity field are due to insufficient correlation coefficients, either values are below the noise level or the surface changed. The noise level is defined as displacement below a significance level of 8 m. Mismatches from surface changes (e.g. due to melting) are excluded by applying a filter based on correlation coefficients and an azimuth range for accepted measurements. At a steep section in the upper part of the glacier tongue, the speed increases to 100 m year^{-1}. Measurements for the periods November 2001–October 2002 and January 2001–October 2002 are too sparse to detect a change in speed at a reliable level.

In general, the glacier characteristics and the results for the glacier tongues in sections E and F (Fig. 7) are similar to the one in section D. The glacier tongue in section E (Rilo Glacier) shows a local speed maximum of about 25–30 m year^{-1} in the middle of the tongue. Maximum speeds of about 50 m year^{-1} are detected for section F (Tshojo Glacier). There appears to be a slight deceleration from the first period (January 2001–November 2001) to the second period (November 2001–October 2002, not shown).

Additional velocity measurements at selected points on some other glaciers in the region under study support the findings presented above, but are not shown and discussed here.

5. Method discussion

Orthoprojection of multi-incidence-angle ASTER images to a combined DEM from SRTM3 and ASTER optical stereo data proves successful. Potential horizontal offsets between the fused data sets are reduced by extracting the ground control points that are necessary for orientation of the ASTER data from the SRTM3 data. We conduct no comparison the SRTM3 georeference and the ASTER image georeference from sensor position and attitude angles (given through the so-called geolocation array in the ASTER header-file; ERSDAC, 1999). Assessment of the accuracy in absolute position is thus not possible. The relative horizontal accuracy of about ±30 m, which is obtained for the transfer of CPs from the SRTM3 DEM to the ASTER images (see section on ASTER DEM generation) points to a consistent georeference throughout the SRTM3 section used.

Filling gaps of the SRTM3 DEM using DEMs derived from ASTER stereo is a suitable technique to obtain a more complete DEM coverage. Since terrain sections that are problematic for the SRTM (e.g. steep slopes and sharp peaks) are often problematic for photogrammetric DEM generation, too, it is preferable to choose coarse but more robust ASTER DEM versions. When using the PCI Orthoengine software, producing ASTER DEMs with different spatial resolutions and comparing the results for gross errors is advisable. In addition, filtering the marked spikes and holes improves the DEMs (Zollinger, 2003). For selected test sites, the SRTM3 DEM shows fewer large

errors than the ASTER DEMs. Therefore, the SRTM3 is used as the master data set and the ASTER DEM is used to fill gaps.

By following the present procedures of multi-sensor DEM generation and fusion, and by evaluating the DEMs through comparison of orthoimages from different incidence angles, a consistent multi-resolution data set of DEMs and repeat orthoimages is compiled using space-derived information only. Sound co-registration and data fusion form the basis for successful matching of horizontal surface displacements from the multitemporal image data.

Feature matching between repeat optical satellite imagery has been mainly conducted on large polar glaciers or ice streams (e.g. Bindschadler et al., 1996; Lefauconnier et al., 1994; Rolstad et al., 1997; Scambos et al., 1992), but is also applicable for smaller mountain glaciers in rough topography. Orthoprojection is a mandatory pre-processing step, necessary to prevent strong topographically induced distortions between the images. Feature tracking techniques are particularly well suited for the Bhutan study area because the cold environment and high basal sliding (see following section) contribute to the preservation of ice surface structures over time. Due to ice melting on the glacier tongues at lower elevation, finding trackable features in these areas is difficult. Significantly fewer corresponding points are obtained for the 2-year period January 2001–October 2002 compared to the 1-year periods in 2001 and 2002 because of surface melt and changes in crevasse patterns.

6. Glaciological interpretation

Glaciers in the southern and central parts of the Himalayas are expected to be especially sensitive to present atmospheric warming due to their summer-accumulation type (Ageta & Higuchi, 1984). An increase in summer air temperature not only enhances ice melt but also significantly reduces the accumulation by altering snowfall to rain. (In contrast, winter-accumulation type glaciers receive their main accumulation at lower temperatures and are thus less sensitive to an increase in air temperature.) Under present climatic conditions, the glacier variations south of the Himalayan main ridge are believed to mainly reflect monsoon dynamics.

Recently, pronounced glacier retreat, with strong regional variability, has been observed in the Himalayas and the Tibet plateau (Fujita et al., 1997; Karma et al., 2003; Li et al., 1998; Ren et al., 2004). In Bhutan, glacier retreat shows a north–south gradient with larger retreat rates in the south (Karma et al., 2003). The influence of the monsoon decreases towards the north of the study area. The continentality of the glaciers increases in the same direction. As a result, the northern glaciers are less sensitive to changes in air temperature and in accumulation during monsoon than the southern ones. The evolution and expansion of glacier lakes in the study area, and the growing hazard from related outbursts is both a clear indicator and a consequence of the glacier shrinkage (Ageta et al., 2000).

The glacier tongues on the northern and southern slope differ in topography and surface characteristic as well as dynamic. The elevation profiles Fig. 8 (cf. Fig. 1 for location) clearly exhibit the topographic difference between the glaciers on the northern and the southern slope of the Himalayan main ridge. The northern glaciers A–C originate from ice plateaus of up to 7000 m, while the southern glaciers originate from steep ice and rock faces. These large head walls provide the sustained supply of rock-debris that covers the southern glaciers, whereas such debris accumulation is not significant for the northern glaciers.

In addition to being debris-covered, the southbound glacier tongues contain thermokarst features such as rapidly changing depressions and supraglacial ponds (Benn et al., 2000; Chikita et al., 1999; Reynolds, 2000). In their terminus zones, glacier speed is near the noise level of the image matching techniques applied, i.e. in the range of 10–20 m year^{-1}. Higher speeds are only reached in steep glacier parts above the tongues.

The northbound glacier tongues show speeds of several tens to over 200 m year^{-1}. These high speeds with steep transverse gradients at the margins imply large amounts of basal sliding. Well preserved crevasses also indicate minimal basal drag.

The northern glaciers have almost no debris cover. Their light-blue ice colour in ASTER VNIR RGB false colour composites—similar to that of cold or polythermal arctic glaciers—indicates a comparably high content of air bubbles refracting the sunlight. The dry-cold continental climate and high elevation of the northern basin suggest the existence of discontinuous permafrost (Brown et al., 2001; Iwata et al., 2003; Xin et al., 1999). In contrast to the southern glaciers, the margins of the northern ones might be frozen to the ground—a fact that is known to favour high subglacial water pressure and may thus enhance basal sliding (e.g. Haeberli & Fisch, 1984; Rabus & Echelmeyer, 1997; Skidmore & Sharp, 1999). The fast-flowing glacier tongues could well reflect the balance velocity, i.e. the ice flux needed to drain the relatively large glacier accumulation areas through the northbound valleys in order to keep the glaciers in geometric equilibrium. More careful examination of this topic requires the (not available) knowledge about

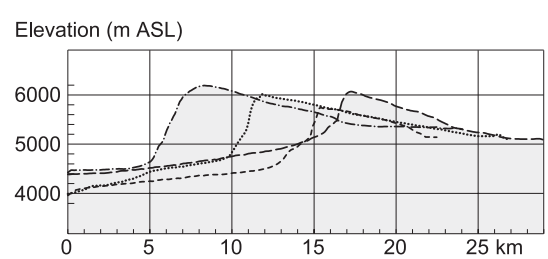

Fig. 8. Surface elevation profiles interpolated from the combined SRTM3-ASTER DEM. Profile locations are indicated in Fig. 1.

the regional precipitation pattern or the horizontal and vertical regional mass balance gradients.

Surface slopes of the southern and northern glacier tongues are both on the order of a few degrees (Fig. 9). For similar slopes, the surface speed is clearly higher for the northern glaciers (Fig. 9). Thus, different surface slopes can largely be excluded as the reason for the large speed differences observed. The speed differences point to different basal processes and higher balance velocities. For the calving glacier tongues, the uniform and relatively high speed might also be linked to an influence of lake water pressure reducing the basal drag.

The low speeds on the southern glacier tongues indicate little supply of ice to large sections of the tongues. Such reduced ice flux supports the development of pronounced differential melt, such as from the evolution of supraglacial ponds and other thermokarst features. The low speeds enhance the accumulation of debris on the glacier surface through reduced debris transport. In summary, the southern tongues appear to be nearly stagnant. The expected present response to atmospheric warming for these glacier tongues is downwasting—essentially decoupled from the dynamics of the upper glacier parts. Under certain topographic circumstances, some southern glacier tongues might even loose contact to the upper glacier parts and become dead ice. As a consequence, enhanced development of glacial lakes on and at the southern glacier tongues, and increase of related hazards has to be expected under conditions of continued atmospheric warming.

In contrast to the southern ones, the northern glacier tongues are fast-flowing. Most likely, these glaciers will dynamically adjust to climate variations and thus respond by retreat to atmospheric warming rather than by local decay. This retreat is enhanced by calving processes where the tongues terminate in lakes. The high ice velocities on the northern glacier tongues are an efficient and thus important component of the ice mass turnover within these glaciers. Therefore, variations of the long-term mass balance of the northern glaciers will be reflected by changes in ice speed. Monitoring the surface velocities from space can thus in particular contribute to assess the behaviour of the northbound glaciers.

If the northern glacier tongues are substantially influenced by the permafrost conditions at their margins, also changes in the ground thermal regime due to atmospheric warming will affect the glacier dynamics. For instance, the basal drag might increase if the possibly frozen glacier margins become temperate and permeable to subglacial water, and the subglacial water pressure decrease therefore.

Through their differences in debris cover and ice velocity, the north- and southbound glaciers play very different roles in the erosion and sediment evacuation within their basins (Benn & Evans, 1998; Hallet et al., 1996; Owen et al., 2003; Shroder & Bishop, 2004). The subglacial abrasion might be enhanced by one order of magnitude underneath the northern glaciers (some tens of mm year^{-1}?) compared to the southern glaciers (some mm year^{-1}?) (Boulton, 1974). The contemporary tectonic uplift in the study region is in the same order of magnitude, a few to over 10 mm year^{-1} (Xu et al., 2000), indicating that spatio-temporal variations in subglacial erosion play an important role in the regional topography evolution. On the southern glaciers, reworking of the supraglacial debris is an important factor of sediment production (Owen et al., 2003). In addition, the southern glaciers, though slow flowing, transfer a significant amount of debris down-valley and thus closer to the rivers where it can be evacuated. In summary, significantly different glacial erosion and sediment evacuation processes and rates might act on both sides of the Bhutan Himalayan main ridge, with potentially important implications for mountain geodynamics (e.g. erosional unloading versus isostatic and/or tectonic uplift), and their dependence on climate forcing and related glacier variations (Bishop et al., 2002, 2003).

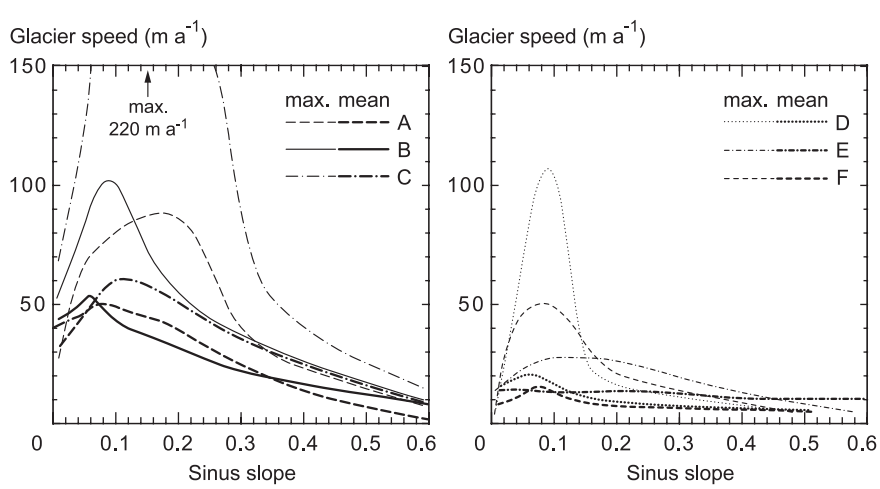

Fig. 9. Surface speed 20 January–20 November 2001 for individual image sections (cf. Fig. 1) as a function of surface slope. Slope is derived from the combined SRTM3-ASTER DEM. Bold lines indicate average, thin lines maximum speeds. Left panel: northern glaciers, right panel: southern glaciers.

The few related studies available for other areas indicate that the glaciers in the southern part of the Bhutan study area are typical for southern and central Himalayan conditions. Heavy debris cover with extensive thermokarst features (e.g. Benn et al., 2000; Chikita et al., 1999; Reynolds, 2000), low ice velocities (e.g. Nakawo et al., 1999; Seko et al., 1998), and similar topographic conditions are also found for other central Himalayan regions. It is not known to us if glaciers draining north into the Tibet plateau in other regions of the Himalayas show also relatively high speeds as found in the present study. However, the study provides the methodology suitable to perform similar investigations along the entire Himalayas (and other mountain ranges).

7. Conclusions and perspectives

This study shows that repeat spaceborne optical data can be used to obtain velocity measurements of remote mountain areas. Data fusion of the SRTM3 DEM and ASTER-derived DEMs is implemented to produce a more complete DEM and orthoimages. This technique minimizes distortion effects from rough topography and allows data from different sensors, orbits and incidence angles to be fused. The procedure can be applied to imagery other than ASTER that we use here (e.g. SPOT 5, Landsat 7 ETM+ pan; Fig. 3; Kääb et al., in press). Development of more sophisticated DEM merging techniques is presently under development.

We explore DEM errors through overlay of orthoimages computed from multi-incidence-angle imagery. Sensors with along-track stereo capability such as ASTER or SPOT 5 are particularly promising candidates for this DEM evaluation method. For known projection geometry, the resulting planimetric differences may also be measured and re-projected in order to refine the underlying DEM (Georgopoulos & Skarlatos, 2003; Kaufmann & Ladstädter, 2002; Norvelle, 1996).

The approach presented here opens new perspectives for observing and understanding spatio-temporal variability of glacier speed between different glaciers. Fresh insight into the topographic, climatic and geologic control of glacier dynamics can be gained from regional-scale comparisons. Studies like the present one will help quantify contemporary glacial erosion and better understand its contribution to the evolution of mountain topography.

It is now feasible to include glacier speed as a parameter in satellite-derived glacier inventories (e.g. GLIMS project "glacier speed inventorying"; Raup et al., 2001). This data could help assess the potential response of individual glaciers to climate change and understand the coupling of glacier dynamics and surface structure. However, comprehensive goals and strategies for glacier speed inventorying have yet to be developed.

The results of the present study underline that space-based remote sensing can provide new insights into the magnitude of selected surface processes and feedback mechanisms that govern mountain geodynamics. Space-based sensors open up a new dimension to studying Earth surface processes in mountain environments.

Acknowledgements

Special thanks are due to Michael Bishop and two anonymous referees for their particularly thorough and helpful comments to this paper. Wilfried Haeberli gave valuable support to this study, and Susan Braun-Clarke edited the English of an earlier version of the manuscript. We are grateful to Tobias Kellenberger and the system administration team of the Department of Geography, University of Zurich, for maintaining the satellite data processing software used. The ASTER scenes applied in this study were provided within the framework of the Global Land Ice Measurements from Space project (GLIMS) through the EROS data center, and are courtesy of NASA/GSFC/METI/ERSDAC/JAROS, and the US/Japan ASTER science team.

References

Ageta, Y., & Higuchi, K. (1984). Estimation of mass balance components of a summer accumulation-type glacier in the Nepal Himalaya. *Geografiska Annaler*, *66A*, 249–255.

Ageta, Y., Iwata, S., Yabuki, H., Naito, N., Sakai, A., Narama, C., et al. (2000). Expansion of glacier lakes in recent decades in the Bhutan Himalayas. In M. Nakawo, C. F. Raymond, & A. Fountain (Eds.), *Debris-Covered Glaciers*, *vol. 264* (pp. 165–175). IAHS Publications.

Aniello, P. (2003). Using ASTER DEMs to produce IKONOS orthophotos. *Earth Observation Magazine*, *12*(5), 22–26.

Baltsavias, E. P. (1996). Digital ortho-images—a powerful tool for the extraction of spatial- and geo-information. *ISPRS Journal of Photogrammetry and Remote Sensing*, *51*(2), 63–77.

Benn, D. I., & Evans, D. J. A. (1998). Glaciers and glaciations. London: Arnold. 734 pp.

Benn, D. I., Wiseman, S., & Warren, C. R. (2000). Rapid growth of a supraglacial lake, Ngozumpa Glacier, Khumbu Himal, Nepal. In M. Nakawo, C. F. Raymond, & A. Fountain (Eds.), *Debris-Covered Glaciers*, *vol. 264* (pp. 177–185). IAHS publications.

Bindschadler, R. A., Fahnestock, M. A., Skvarca, P., & Scambos, T. A. (1994). Surface-velocity field of the northern Larsen Ice Shelf, Antarctica. *Annals of Glaciology*, *20*, 319–326.

Bindschadler, R., Vornberger, P., Blankenship, D., Scambos, T., & Jacobel, R. (1996). Surface velocity and mass balance of Ice Streams D and E, West Antarctica. *Journal of Glaciology*, *42*(142), 461–475.

Bishop, M. P., Shroder Jr., J. F., Bonk, R., & Olsenholler, J. (2002). Geomorphic change in high mountains: A western Himalayan perspective. *Global and Planetary Change*, *32*(4), 311–329.

Bishop, M. P., Shroder Jr., J. F., & Colby, J. D. (2003). Remote sensing and geomorphometry for studying relief production in high mountains. *Geomorphology*, *55*(1–4), 345–361.

Bishop, M. P., et al. (2004). Global land ice measurements from space (GLIMS): Remote sensing and GIS investigations of the Earth's Cryosphere. *Geocarto International*, *19*(2), 57–84.

Boulton, G. S. (1974). Processes and patterns of subglacial erosion. In D. R. Coates (Ed.), *Glacial geomorphology* (pp. 47–87). Binghamton: State University of New York.

Brown, J., Ferrians Jr., O. J., Heginbottom, J. A., & Melnikov, E. S. (2001). Circum-arctic map of permafrost and ground ice conditions. *National snow and ice data center/world data center for glaciology*. Boulder, CO: Digital media.

Chikita, K., Jha, J., & Yamada, T. (1999). Hydrodynamics of a supraglacial lake and its effect on the basin expansion: Tsho Rolpa, Rolwaling valley, Nepal Himalaya. *Arctic, Antarctic, and Alpine Research*, *31*, 58–70.

ERSDAC. (1999). ASTER User's Guide. Parts I and II, Earth Remote Sensing Data Analysis Center, Tokyo, Japan.

Evans, A. N. (2000). Glacier surface motion computation from digital image sequences. *IEEE Transactions on Geoscience and Remote Sensing*, *38*(2), 1064–1072.

Frezzotti, M., Capra, A., & Vittuari, L. (1998). Comparison between glacier ice velocities inferred from GPS and sequential satellite images. *Annals of Glaciology*, *27*, 54–60.

Fujita, K., Nakawo, M., Fujii, Y., & Paudyal, P. (1997). Changes in glaciers in Hidden valley, Mukut Himal, Nepal Himalayas, from 1974 to 1994. *Journal of Glaciology*, *43*, 583–588.

Gansser, A. (1970). Lunana, the peaks, glaciers and lakes of northern Bhutan. *The Mountain World, Schweizerische Stiftung für Alpine Forschungen* (pp. 117–131).

Georgopoulos, A., & Skarlatos, D. (2003). A novel method for automating the checking and correction of digital elevation models using orthophotographs. *Photogrammetric Record*, *18*(102), 156–163.

Haeberli, W., & Fisch, W. (1984). Electrical resistivity soundings of glacier beds: A test study on Grubengletscher, Wallis, Swiss Alps. *Journal of Glaciology*, *30*(106), 373–376.

Hallet, B., Hunter, L., & Bogen, J. (1996). Rates of erosion and sediment evacuation by glaciers: A review of field data and their implications. *Global and Planetary Change*, *12*, 213–235.

Hirano, A., Welch, R., & Lang, H. (2003). Mapping from ASTER stereo image data: DEM validation and accuracy assessment. *ISPRS Journal of Photogrammetry and Remote Sensing*, *57*(5–6), 356–370.

Iwata, S., Naito, N., Narama, C., & Karma (2003). Rock glaciers and the lower limit of mountain permafrost in the Bhutan Himalayas. *Zeitschrift für Geomorphologie. Supplementband*, *130*, 129–143.

Kääb, A. (2002). Monitoring high-mountain terrain deformation from air- and spaceborne optical data: Examples using digital aerial imagery and ASTER data. *ISPRS Journal of Photogrammetry and Remote Sensing*, *57*(1–2), 39–52.

Kääb, A. (2004). *Mountain glaciers and permafrost creep. Methodical research perspectives from earth observation and geoinformatics technologies*. Habilitation thesis, Department of Geography, University of Zurich. 205 pp.

Kääb, A., Huggel, C., Paul, F., Wessels, R., Raup, B., Kieffer, H., et al. (2003a). Glacier monitoring from ASTER imagery: Accuracy and applications. *EARSel eProceedings*, *2*, 43–53.

Kääb, A., Isakowski, Y., Paul, F., Neumann, A., & Winter, R. (2003b). Glaziale und periglaziale Prozesse: Von der statischen zur dynamischen Visualisierung. *Kartographische Nachrichten*, *53*(5), 206–212.

Kääb, A., Lefauconnier, B., & Melvold, K. (2004). Flow field of Kronebreen, Svalbard, using repeated Landsat7 and ASTER data. *Annals of Glaciology*, *42* (in press).

Kääb, A., Reynolds, J. M., & Haeberli, W. (2005). Glacier and permafrost hazards in high mountains. In U. M. Huber, H. K. M. Bugmann, & M. A. Reasoner (Eds.), *Global change and mountain regions: A state of knowledge overview. Advances in Global Change Research* (pp. 225–234). Dordrecht: Springer.

Kääb, A., & Vollmer, M. (2000). Surface geometry, thickness changes and flow fields on creeping mountain permafrost: Automatic extraction by digital image analysis. *Permafrost and Periglacial Processes*, *11*(4), 315–326.

Kääb, A., Wessels, R., Haeberli, W., Huggel, C., Kargel, J., & Khalsa, S.J.S. (2003c). Rapid ASTER imaging facilitates timely assessment of glacier hazards and disasters. *EOS Transactions, American Geophysical Union*, *84*(13), 117–121.

Karma, Ageta, Y., Naito, N., Iwata, S., & Yabuki, H. (2003). Glacier distribution in the Himalayas and glacier shrinkage from 1963 to 1993 in the Bhutan Himalayas. *Bulletin of Glaciological Research*, *20*, 29–40.

Kaufmann, V., & Ladstädter, R. (2002). Spatio-temporal analysis of the dynamic behaviour of the Hochebenkar rock glaciers (Oetztal Alps, Austria) by means of digital photogrammetric methods. *Grazer Schriften der Geographie und Raumforschung*, *37*, 119–140.

Kieffer, H. H. et al. (2000). New eyes in the sky measure glaciers and ice sheets. *EOS Transactions, American Geophysical Union, 81*(24), 265, 270–271.

Lefauconnier, B., Hagen, J. O., & Rudant, J. P. (1994). Flow speed and calving rate of Kronebreen glacier, Svalbard, using SPOT images. *Polar Research*, *13*(1), 59–65.

Li, Z., Sun, W., & Zeng, Q. (1998). Measurements of glacier variation in the Tibetan Plateau using Landsat data. *Remote Sensing of Environment*, *63*, 258–264.

Lucchitta, B. K., & Ferguson, H. M. (1986). Antarctica—measuring glacier velocity from satellite images. *Science*, *234*(4780), 1105–1108.

McCarthy, J. J., Canziani, O. F., Leary, N. A., Dokken, D. J., & White, K. S. (Eds.). (2001). *Contribution of working group II to the third assessment report of the intergovernmental panel on climate change (IPCC)* (pp. 170). UK: Cambridge University Press. 1000 pp.

Meyer, M., Haslinger, E., Häusler, H., Leber, D., & Wangda, D. (2003). The glacial chronology of eastern Lunana (NW Bhutan—Himalaya). *Abstracts, 16th INQUA Congress*. *Abstract*, *No. 54-10* (p. 170). Reno: The Desert Research Institute.

Mool, P. K., Wangda, D., Bajrachary, S. R., Kunzang, K., Gurung, D. R., & Joshi, S. P. (2001). Inventory of glaciers, glacial lakes and glacial lake outburst floods. Bhutan. International Centre for Integrated Mountain Development, Kathmandu, Nepal. 227 pp.

Nakawo, M., Yabuki, H., & Sakai, A. (1999). Characteristics of Khumbu Glacier, Nepal Himalaya: Recent change in the debris-covered area. *Annals of Glaciology*, *28*, 118–122.

Norvelle, R. (1996). Using iterative orthophoto refinements to generate and correct digital elevation models (DEM's). *Digital Photogrammetry: An Addendum to the Manual of Photogrammetry* (pp. 151–155). Falls Church: American Society of Photogrammetry and Remote Sensing.

Owen, L. A., Derbyshire, E., & Scott, C. H. (2003). Contemporary sediment production and transfer in high-altitude glaciers. *Sedimentary Geology*, *155*, 13–36.

Paul, F., Kääb, A., Maisch, M., Kellenberger, T., & Haeberli, W. (2004). Rapid disintegration of Alpine glaciers observed with satellite data. *Geophysical Research Letters*, *31*, L21402, doi:10.1029/2004GL020816.

Rabus, B., Eineder, M., Roth, A., & Bamler, R. (2003). The shuttle radar topography mission—a new class of digital elevation models acquired by spaceborne radar. *ISPRS Journal of Photogrammetry and Remote Sensing*, *57*(4), 241–262.

Rabus, B. T., & Echelmeyer, K. A. (1997). The flow of a polythermal glacier: McCall Glacier, Alaska, USA. *Journal of Glaciology*, *43*(145), 522–536.

Raup, B., Scharfen, G., Khalsa, S., & Kääb, A. (2001). The design of the GLIMS (Global Land Ice Measurements from Space) glacier database. *EOS Transactions Supplement, American Geophysical Society*, *82*(47) (full Meeting Supplement, Abstract IP41A-12).

Ren, J., Qin, D., Kang, S., Hou, S., Pu, J., & Jing, Z. (2004). *Glacier variations and climate warming and drying in the central Himalayas*. *Chinese Science Bulletin*, *49*(1), 65–69.

Reynolds, J. M. (2000). On the formation of supraglacial lakes on debris-covered glaciers. In M. Nakawo, C. F. Raymond, & A. Fountain (Eds.), *Debris-Covered Glaciers*, *vol. 264* (pp. 153–161). IAHS publications.

Rignot, E., Forster, R., & Isacks, B. (1996). Interferometric radar observations of Glaciar San Rafael, Chile. *Journal of Glaciology*, *42*(141), 279–291.

Rignot, E., Rivera, A., & Casassa, G. (2003). Contribution of the Patagonia Icefields of South America to sea level rise. *Science*, *302*, 434–437.

Rivera, A., Casassa, G., Bamber, J., & Kääb, A. (2003). Ice elevation changes in the Southern Patagonia Icefield, using ASTER DEMs, aerial photographs and GPS data. *Journal of Glaciology* (in press).

Rolstad, C., Amlien, J., Hagen, J. O., & Lundén, B. (1997). Visible and near-infrared digital images for determination of ice velocities and surface elevation during a surge on Osbornebreen, a tidewater glacier in Svalbard. *Annals of Glaciology*, *24*, 255–261.

Scambos, T. A., Dutkiewicz, M. J., Wilson, J. C., & Bindschadler, R. A. (1992). Application of image cross-correlation to the measurement of glacier velocity using satellite image data. *Remote Sensing of Environment*, *42*(3), 177–186.

Seko, K., Yakubi, H., Nakawo, M., Sakai, A., Kadota, T., & Yamada, Y. (1998). Changing surface features of Khumbu glacier, Nepal Himalayas revealed by SPOT images. *Bulletin of Glacier Research*, *16*, 33–41.

Shroder Jr., J. F., & Bishop, M. P. (2004). Mountain geomorphic systems. In M. P. Bishop, & J. F. Shroder Jr. (Eds.), *Geographic information science and mountain geomorphology* (pp. 33–73). Praxis, Chichester, UK: Springer.

Skidmore, M. L., & Sharp, M. J. (1999). Drainage system behaviour of a High-Arctic polythermal glacier. *Annals of Glaciology*, *28*, 209–215.

Skvarca, P., Raup, B., & De Angelis, H. (2003). Recent behaviour of Glaciar Upsala, a fast-flowing calving glacier in Lago Argentino, southern Patagonia. *Annals of Glaciology*, *36*, 184–188.

Strozzi, T., Kääb, A., & Frauenfelder, R. (2004). Detecting and quantifying mountain permafrost creep from in-situ, airborne and spaceborne remote sensing methods. *International Journal of Remote Sensing*, *25*(15), 2919–2931.

Strozzi, T., Wegmüller, U., Wiesmann, A., & Werner, C. (2003). Validation of the X-SAR SRTM DEM for ERS and JERS SAR geocoding and 2-pass differential interferometry in alpine regions. *Proceedings, IGARSS'03,* Toulouse, France.

Sun, G., Ranson, K. J., Kharuk, V. I., & Kovacs, K. (2003). Validation of surface height from Shuttle Radar Topography Mission using Shuttle laser altimeter. *Remote Sensing of Environment*, *88*(4), 401–411.

Toutin, T. (2002). Three-dimensional topographic mapping with ASTER stereo data in rugged topography. *IEEE Transactions on Geoscience and Remote Sensing*, *40*(10), 2241–2247.

Toutin, T., & Cheng, P. (2001). DEM generation with ASTER stereo data. *Earth Observation Magazine*, *10*(6), 10–13.

Van Zyl, J. J. (2001). The Shuttle Radar Topography Mission (SRTM): a breakthrough in remote sensing of topography. *Acta Astronautica*, *48*(5–12), 559–565.

Watanabe, T., & Rothacher, D. (1996). The 1994 Lugge Tsho glacial lake outburst flood, Bhutan Himalaya. *Mountain Research and Development*, *16*, 77–81.

Whillans, I. M., & Tseng, Y. -H. (1995). Automatic tracking of crevasses on satellite images. *Cold Regions Science and Technology*, *23*(2), 201–214.

Xin, L., Guodong, C., Qingbai, W., & Yongjian, D. (1999). Chinese cryospheric information system. *Proceedings, The 20th Asian Conference on Remote Sensing,* Hong Kong.

Xu, C., Liu, J., Song, C., Jiang, W., & Shi, C. (2000). GPS measurements of present-day uplift in the Southern Tibet. *Earth, Planets and Space*, *52*(10), 735–739.

Zollinger, S. (2003). *ASTER satellite data for automatic generation of DEMs in high mountains. Mt. Everest region*. Diploma thesis (in German), Department of Geography, University of Zurich.